

Near room-temperature ferromagnetism from double exchange in the van der Waals material CrGeTe₃: Evidence from optical conductivity under pressure

Jihaan Ebad-Allah^{1,2}, Daniel Guterding³, Meera Varma,¹ Mangesh Diware^{3,4}, Shraddha Ganorkar⁵, Harald O. Jeschke⁶, and Christine A. Kuntscher¹

¹Experimentalphysik II, Institute for Physics, University of Augsburg, 86135 Augsburg, Germany

²Department of Physics, Tanta University, 31527 Tanta, Egypt

³Technische Hochschule Brandenburg, Magdeburger Straße 50, 14770 Brandenburg an der Havel, Germany

⁴Advanced Research Division, Park Systems Co., Suwon 16229, Republic of Korea

⁵School of Mechanical Engineering, Sungkyunkwan University, 2066 Seobu-ro, Jangan-gu, Suwon, Gyeonggi-do 16419, Republic of Korea

⁶Research Institute for Interdisciplinary Science, Okayama University, Okayama 700-8530, Japan



(Received 17 September 2024; accepted 3 March 2025; published 1 April 2025)

The unexpected discovery of intrinsic ferromagnetism in layered van der Waals materials has sparked interest in both their fundamental properties and their potential for novel applications. Recent studies suggest near room-temperature ferromagnetism in the pressurized van der Waals crystal CrGeTe₃. We perform a comprehensive experimental and theoretical investigation of magnetism and electronic correlations in CrGeTe₃, combining broad-frequency reflectivity measurements with density functional theory and dynamical mean-field theory calculations. Our experimental optical conductivity spectra trace the signatures of developing ferromagnetic order and of the insulator-to-metal transition (IMT) as a function of temperature and hydrostatic pressure. With increasing pressure, we observe the emergence of a midinfrared feature in the optical conductivity, indicating the development of strong orbital-selective correlations in the high-pressure ferromagnetic phase. We find a distinct relationship between the plasma frequency and Curie temperature of CrGeTe₃, which strongly suggests that a double-exchange mechanism is responsible for the observed near room-temperature ferromagnetism. Our results clearly demonstrate the existence of a charge-transfer gap in the metallic phase, ruling out its previously conjectured collapse under pressure.

DOI: 10.1103/PhysRevB.111.L140402

Layered transition-metal chalcogenides host a variety of interesting physical properties and exotic phases such as charge-density wave [1], Mott insulator [2–5], superconductor [6–8], antiferromagnetic topological insulator [9–12], Weyl semimetal [13–15], ferromagnetic (FM) nodal-line semimetal [16–19], and topological magnon insulator [20–22], which emerge due to electronic correlations and nontrivial topology in these materials. Furthermore, two-dimensional (2D) transition-metal chalcogenides provide an ideal platform for realizing atomically thin van der Waals (vdW) crystals with unique properties such as 2D ferromagnetism [23,24] or topological quantum spin Hall effect [25,26], as well as excellent prospects for novel applications [27–30].

The 2D vdW transition-metal trichalcogenide CrGeTe₃ and its sibling CrSiTe₃ are prominent examples for such materials [20,31–33], especially since the discovery of long-range FM order in few-layer CrGeTe₃ [23]. Each layer of this material forms a honeycomb network of edge-sharing octahedra with a central Cr atom bonded to six Te atoms [34,35], as illustrated in the Supplemental Material Ref. [36] (see also Refs. [37–82] therein). At ambient pressure, CrGeTe₃ is a charge-transfer insulator with an energy gap between 0.2 and 0.7 eV [35,83,84]. It shows FM order below the Curie temperature $T_C = 61\text{--}67\text{ K}$ [35,37,85].

The generally weak vdW forces between layers make these materials susceptible to tuning by application of external pressure, which may lead to structural, magnetic, or

purely electronic phase transitions [33,37,51,86–88]. Recent transport studies revealed that CrGeTe₃ is indeed sensitive to external pressure, which leads to a correlated metallic state and near room-temperature ferromagnetism above ~ 3 GPa [37,40]. X-ray diffraction and Raman scattering studies show the absence of a structural phase transition in CrGeTe₃ up to 10 GPa [89]. Furthermore, electron doping via chemical intercalation [90] or electrostatic gating [30], tensile strain via heterostructuring [91–93], and amorphization due to irradiation [94] all lead to greatly enhanced Curie temperatures in CrGeTe₃.

Naturally, this has led to a debate on the mechanism responsible for the enhanced T_C . While the ferromagnetism of pristine CrGeTe₃ at ambient pressure has been conclusively attributed to FM superexchange [38,39], the situation is less clear for the aforementioned modifications. Some authors explain the increase in Curie temperature with the onset of double-exchange interactions upon electron doping [30,90], while another study reports a rise in T_C upon hole doping [94]. Yet another study attributes the rise in T_C upon lattice expansion to a weakening of competing antiferromagnetic exchange paths [91]. Under pressure, the increase in Curie temperature has been explained in terms of a decreasing charge-transfer gap, which may enhance FM superexchange [37], while we could not definitively pin down the mechanism of enhanced T_C in our previous theoretical study [40].

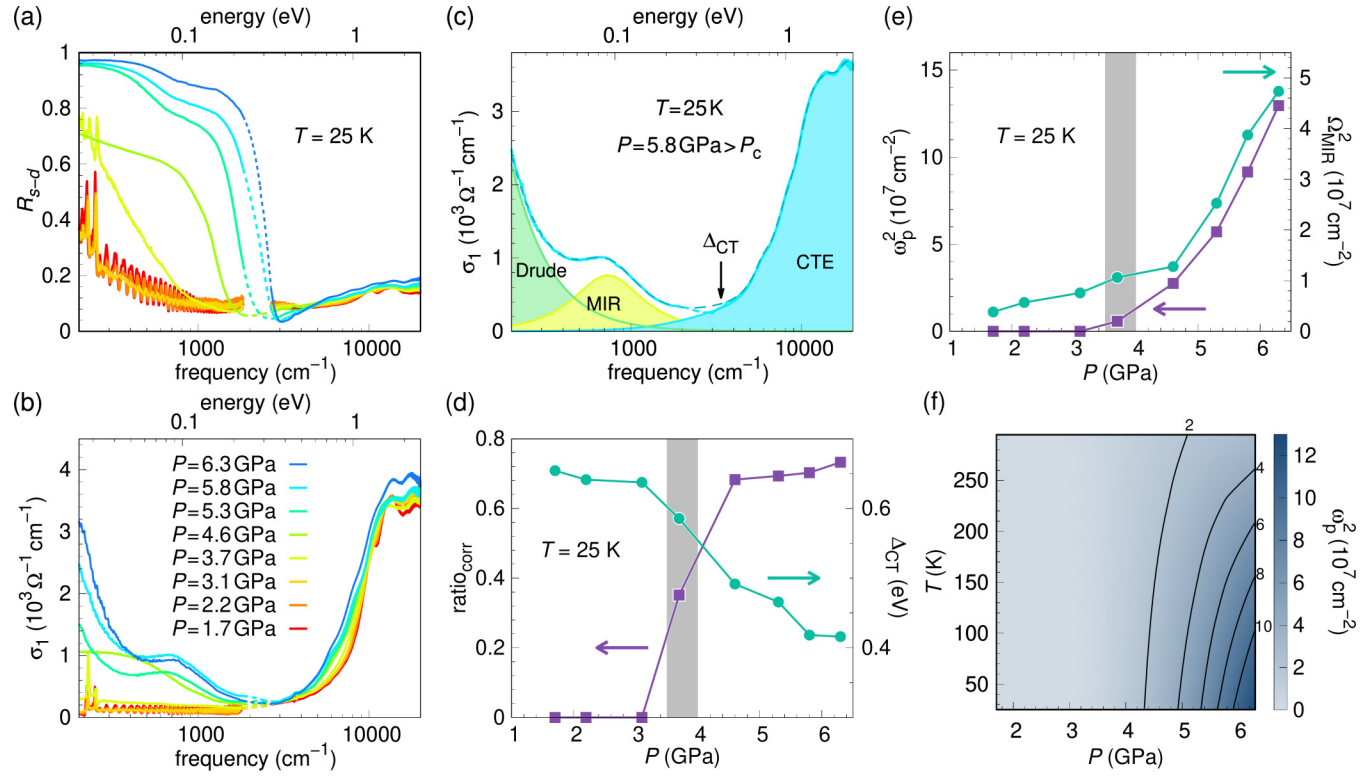


FIG. 1. Pressure-dependent (a) reflectivity R_{s-d} and (b) real part of the optical conductivity σ_1 of CrGeTe_3 at 25 K. (c) Optical conductivity spectrum at 25 K and 5.8 GPa together with the Drude-Lorentz fit and contributions. The charge-transfer gap Δ_{CT} is indicated by the arrow. (d) Pressure-dependent correlation ratio $\text{ratio}_{\text{corr}}$ (see text for definition) and charge-transfer gap size Δ_{CT} , all at 25 K. (e) Pressure-dependent Drude oscillator strength ω_p^2 and oscillator strength Ω_{MIR}^2 of the MIR band, all at 25 K. The vertical gray bar in (d) and (e) indicates the critical pressure P_c of the IMT. (f) Contour map of Drude oscillator strength ω_p^2 .

In the present study we attempt to resolve this controversy by analyzing the optical conductivity of the vdW ferromagnet CrGeTe_3 under hydrostatic pressure in a combined experimental and theoretical approach. Using broad-frequency reflectivity measurements as well as density functional theory (DFT) and dynamical mean-field theory (DMFT) calculations, we clarify the effect of both magnetism and electronic correlations on the electrodynamic response across the insulator-to-metal transition (IMT). Our optical conductivity measurements show clear signatures of developing FM order as a function of temperature and pressure. In the high-pressure metallic phase, a midinfrared (MIR) feature emerges in the optical conductivity, which we can attribute to strong orbital-selective electronic correlations. Our data unveils a distinct relationship between the observed plasma frequency ω_p and the ordering temperature T_C of CrGeTe_3 , which clearly points to a double-exchange mechanism [78]. Our data show that the optical gap persists into the metallic phase, ruling out a previously conjectured collapse of the charge-transfer gap under pressure [37]. This, however, does not exclude the relevance of FM superexchange under pressure (see Ref. [36]). Our study highlights the intertwined nature of magnetism and electronic correlations in CrGeTe_3 .

We obtain the optical conductivity spectrum throughout the pressure-temperature phase diagram of CrGeTe_3 by measuring the reflectivity of a small piece of single crystal, loaded into a diamond anvil pressure cell, using Fourier-transform

infrared spectroscopy at cryogenic temperatures (see Ref. [36] for details). The reflectivity R_{s-d} of CrGeTe_3 at 25 K is displayed in Fig. 1(a) for selected pressures. Up to 3.1 GPa, the overall reflectivity spectrum changes only modestly. For pressures of 3.7 GPa and above, the low-energy part (below 0.37 eV, i.e., 3000 cm\$^{-1}\$) of R_{s-d} changes drastically: Fabry-Perot interference disappears, the reflectivity level suddenly increases, phonon modes assigned to Te-Cr-Te bending and Cr-Te stretching modes are screened, and a plasma edge develops above 4.6 GPa. Further application of pressure continuously increases the low-energy reflectivity level, while the plasma edge becomes more distinct and shifts to higher energies. Interestingly, a steplike plateau related to an MIR band (see below) develops below the plasma edge. The above observations are evidence of a pressure-induced IMT, consistent with recent reports [37,40,95]. We note here that the critical pressure of the IMT in our study (3.7 GPa) is slightly lower than the one reported in Ref. [37] (7 GPa), but in very good agreement with recent electrical transport studies [95,96].

The signatures of the IMT are also revealed in the real part of the optical conductivity σ_1 [see Fig. 1(b)], obtained from the R_{s-d} spectra via Kramers-Kronig analysis. For pressures below 3.7 GPa, σ_1 consists of three pronounced high energy excitations at around 2.1, 1.6, and 1.3 eV [L5, L4, and L6 excitations, respectively, in Fig. 2(d)], followed toward lower energies by a drop, marking an absorption edge at ~ 0.65 eV, and two phonon modes at around 0.032 and 0.027 eV. The

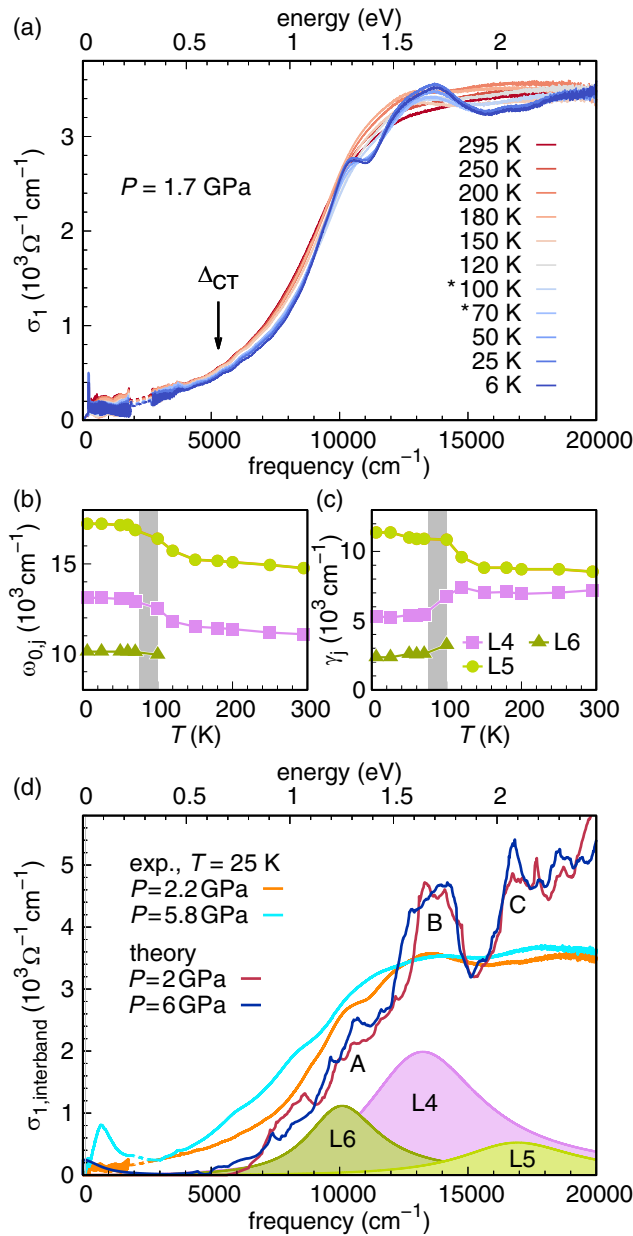


FIG. 2. (a) Optical conductivity σ_1 of CrGeTe_3 at 1.7 GPa at selected temperatures. The magnetic onset temperature is identified by the asterisks. (b) Frequency position and (c) width (γ) of the L4, L5, and L6 excitations, as obtained from Lorentz fits at 1.6 GPa as a function of temperature T . The vertical gray bar in (b) and (c) indicates the Curie temperature T_C . (d) Comparison between the experimental and theoretical interband conductivity $\sigma_{1,\text{interband}}$ at 25 K , i.e., within the ferromagnetic phase, together with the fit contributions L4, L5, and L6 at 2.2 GPa .

phonon modes exhibit only minor changes, either by pressure or temperature, and could be assigned to Te-Cr-Te bending and Cr-Te stretching modes, as in CrSiTe_3 [97]. The absence of the Drude term in the low-pressure regime confirms the ambient-pressure insulating phase, consistent with previous reports [37,40,95]. From the energy position of the absorption edge, we can also estimate the charge-transfer gap size Δ_{CT} (see Ref. [36] for details), depicted in Fig. 1(d) as a function

of pressure at 25 K . Accordingly, the charge-transfer gap is almost constant up to $\sim 3 \text{ GPa}$, whereas above $\sim 3 \text{ GPa}$ it starts to decrease in a moderate fashion.

Above the critical pressure $P_c \approx 3.7 \text{ GPa}$, we need to include a Drude term into the fitting model for the optical response to account for the presence of itinerant charge carriers. With this Drude term, the model captures the sudden increase in the low-energy region of σ_1 [see Fig. 1(c) as an example], consistent with the recently reported increase in carrier concentration under pressure [95]. Within the metallic regime, the Drude oscillator strength ω_p^2 , which is the square of the plasma frequency ω_p , increases with increasing pressure [see Fig. 1(e)]. ω_p^2 serves as a measure to trace the metallic regions in the pressure-temperature phase diagram of CrGeTe_3 depicted in Fig. 1(f).

The presence of itinerant charge carriers leads to a screening of the low-frequency phonon modes. Additionally, an absorption band appears at $\sim 0.09 \text{ eV}$ (MIR band) [see Fig. 1(c)] and its oscillator strength Ω_{MIR}^2 increases with pressure, as shown in Fig. 1(e). Simultaneously, the charge-transfer gap Δ_{CT} suddenly shrinks around P_c [see Fig. 1(d)], indicating major changes in the electronic band structure. The charge-transfer gap is slightly reduced from ~ 0.65 to 0.4 eV , but does not close even at the highest measured pressure, consistent with our theoretical calculations (see Ref. [36]). A finite Δ_{CT} in the metallic state contradicts the assumptions made in Ref. [37], where the onset of metallicity in CrGeTe_3 at $\sim 7 \text{ GPa}$ was ascribed to the collapse of the charge-transfer gap boosting the interlayer ferromagnetic superexchange interaction.

Next, we focus on the effect of pressure on the magnetic ordering in CrGeTe_3 , as revealed by the temperature-induced changes in the optical response at 1.7 GPa [insulating phase, see Fig. 2(a)] and 5.8 GPa [metallic phase, see Fig. 3(a)]. At 1.7 GPa , significant changes upon cooling occur in the high-energy excitations (above $\sim 0.7 \text{ eV}$) in the temperature range 70 – 100 K (see also Ref. [36]). A decomposition of the optical spectra reveals an anomaly in the frequency position and width (γ) of the L4 and L5 Lorentz oscillators and the appearance of the L6 excitation during cooling down below 100 K , as displayed by the vertical gray bar in Figs. 2(b) and 2(c). The appearance of an additional excitation could also be due to a splitting of the L4 excitation.

We interpret these excitations in the optical conductivity spectra and their pressure-induced changes using density functional theory (DFT) calculations of electronic band structure and optical conductivity (see Ref. [36] for details). Figure 2(d) displays the pressure evolution of the interband optical conductivity $\sigma_{1,\text{interband}}$ in the experiment (at 25 K and after subtracting the Drude term) and our DFT calculations. The theoretical calculations agree well with the experimental interband conductivity spectra [see Fig. 2(d)]. In particular, the charge-transfer gap does not close even at the highest studied pressure (6 GPa), which is also supported by the high-pressure electronic band structure (see Ref. [36]).

The experimental optical conductivity at 25 K contains three prominent features [see Fig. 2(d)] at around 1.3 eV (A), 1.6 eV (B), and 2.1 eV (C). The main three features A, B, and C can be explained based on our DFT calculations. The density of states is dominated by Cr $3d$ and Te $5p$ orbitals. Te and

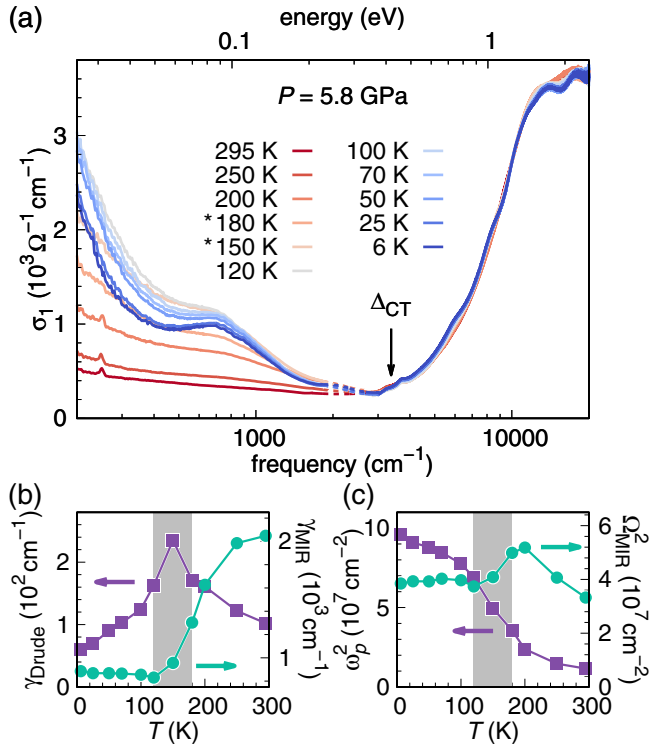


FIG. 3. (a) Optical conductivity σ_1 of CrGeTe₃ at 5.8 GPa at selected temperatures. The magnetic onset temperature is identified by the asterisks. (b) Width and (c) oscillator strength of the Drude term and the MIR oscillator at 5.8 GPa as a function of temperature. The vertical gray bars in (b) and (c) indicate the Curie temperature T_C .

Ge states are present for both the majority and minority spins. The Cr 3d orbitals are spin split and mostly occupied for the majority spin, while being mostly unoccupied for the minority spin. This occupation pattern due to ferromagnetic ordering generates the specific three-peak structure of Fig. 2(d), which is nearly unaffected by pressure. For a more detailed analysis see Ref. [36].

At 5.8 GPa (metallic phase), the high-energy excitations are affected similarly when cooling down, though the temperature-induced changes are less pronounced and occur already at a higher temperature of ~ 150 K (see Fig. 3(a) and Ref. [36]). The effect of magnetic ordering on the low-energy Drude and MIR features upon cooling is, however, remarkably strong: At around 150 K the Drude width shows a maximum and its oscillator strength drastically increases with further cooling. The MIR band sharpens and shows anomalous behavior in its oscillator strength [see Figs. 3(b) and 3(c)]. Two main conclusions can thus be drawn from our optical data: (i) the FM transition temperature is increased by pressure, consistent with Ref. [37], and (ii) the FM ordering strongly affects the optical response. The latter effect is very rare and, according to our knowledge, has been observed up to now only in FM manganese perovskites [98–100] and the FM hexaboride EuB₆ [101,102].

In our previous DFT+DMFT calculations [40] we observed nearly momentum independent features of the Cr 3d_{z²} spectral function about 200 meV above (minority spin) and below (majority spin) the Fermi level at $P = 5$ GPa, which

are created by electron-electron correlations (see Ref. [36]). The MIR feature is explained by an optical transition between the Te 5p states at the Fermi level to these Cr 3d_{z²} minority spin states about 200 meV above the Fermi level, and is thus a signature of electronic correlations in the metallic phase. Based on our DFT+DMFT calculations we also extracted orbital-resolved mass enhancements, which are strongly differentiated with respect to the orbital and spin species, with Cr 3d_{z²} electrons being by far the most strongly correlated. Our orbital-averaged experimental estimate of the mass enhancement 1/ratio_{corr} $\approx 1/0.7 \approx 1.4$ gives similar results (see Fig. 1(d) and Ref. [36]). Accordingly, the metallic phase of FM CrGeTe₃ is moderately correlated. In comparison with other vdW materials, the correlation strength is similar to that of transition metal dichalcogenides [62–64], but significantly weaker than in FM CrI₃ monolayers [67] (see Table S1 in Ref. [36]).

X-ray absorption (XAS) and x-ray magnetic circular dichroism (XMCD) measurements for CrGeTe₃ at ambient pressure point to a mixed ground state of Cr³⁺ and Cr²⁺ states due to hybridization between Cr and Te [38]. Consistent with these findings, our previous calculations [40] showed a Cr magnetic moment slightly above $3\mu_B$ at ambient pressure, which decreases toward $2.5\mu_B$ at around $P = 10$ GPa due to the appearance of both holes in the majority spin Cr 3d orbitals and electrons in the minority spin Cr 3d orbitals. Such a decrease of magnetic moments under pressure is also seen experimentally [37]. This suggests that the valence fluctuations of Cr under pressure also include Cr⁴⁺ states.

While these considerations already suggest that a double-exchange mechanism may be responsible for the sharp increase of the Curie temperature in the metallic phase, our experimental determination of the squared plasma frequency reveals a distinct enhancement in the metallic phase [see Fig. 1(e)]. A mean-field study [78] of the double-exchange Hamiltonian [79] shows that the Curie temperature T_C should be a linear function of the squared plasma frequency ω_p^2 in double-exchange magnets. In the metallic phase of CrGeTe₃, this relation is in excellent agreement with our data and those of Ref. [37] [see Fig. 4(b)]. By matching the values of the plasma frequency back to the pressure axis, we obtain Fig. 4(c), which shows that the double-exchange model accurately describes the rise in Curie temperature upon entering the metallic phase.

Magnetism and correlations in CrGeTe₃ are intertwined and strongly differentiated by orbital and spin. Due to the trigonal crystal field, the Cr 3d_{z²} orbital has the highest energy of all occupied orbitals in a Cr³⁺ configuration. Therefore, valence fluctuations in CrGeTe₃ mainly affect the Cr 3d_{z²} orbital. In particular, the creation of holes in the majority spin Cr 3d_{z²} orbital enables the double-exchange process, but also affects the behavior of minority spin electrons, which localize around these holes to avoid the Coulomb repulsion of a doubly occupied site (see Ref. [36]). This localization weakens as more holes are created, which contributes to the observed decrease of correlations (increase of ratio_{corr}) with further application of pressure in the metallic phase [see Fig. 1(d)]. The minority spin electrons are nevertheless subject to unfavorable Hund's rule interaction (see Ref. [36]), which we

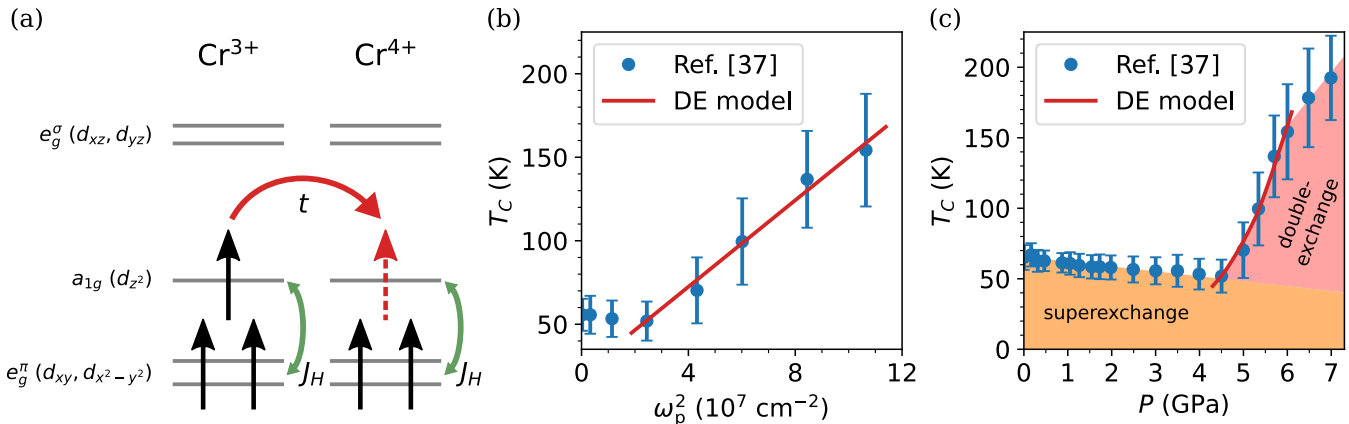


FIG. 4. (a) Schematic depiction of the double-exchange interaction in CrGeTe_3 under high pressure between a d_{z^2} electron on Cr^{3+} and a hole in the d_{z^2} orbital on Cr^{4+} . Black arrows denote majority spins. The red dashed arrow represents the majority spin after it has moved into the hole. Horizontal gray lines represent energy levels of $\text{Cr} 3d$ orbitals. The kinetic term is denoted as t , and J_H is the Hund's coupling. (b) Curie temperature T_C with experimental error bars from Ref. [37] versus the square of the plasma frequency ω_p^2 measured in the present study. The red line represents the linear relationship expected from a double-exchange mechanism in the metallic phase [78]. (c) Curie temperature T_C with experimental error bars from Ref. [37] versus pressure P . The red line represents the Curie temperature T_C expected from a double exchange model based on our experimental plasma frequency ω_p^2 as a function of pressure. The double exchange mechanism clearly explains the increase of the Curie temperature when entering the metallic phase. At present, our data only extend to a pressure of up to 6.3 GPa. Therefore, the extension of double exchange to higher pressures is only a conjecture.

believe leads to the emergence of the MIR feature in the σ_1 spectrum.

In conclusion, our study shows that the optical conductivity of the van der Waals material CrGeTe_3 is strongly affected by ferromagnetic ordering and electronic correlations, while being accurately described by DFT+DMFT calculations. The appearance of an MIR feature in the optical conductivity is linked to the emergence of significant electron-electron correlations upon entering the metallic phase, especially in the $\text{Cr} 3d_{z^2}$ orbital. Based on our measured plasma frequencies, we showed that the increased Curie temperature in the high pressure metallic phase can be explained by a double-exchange mechanism, likely mediated by the pressure-induced creation of holes in the $\text{Cr} 3d_{z^2}$ orbital. The hereby induced valence fluctuations of Cr could be tested by XAS measurements under pressure. Thus, we can resolve the controversy on exchange interactions in CrGeTe_3 under pressure: in the low-pressure insulating regime, FM superexchange dominates, but gradually weakens as pressure causes deviations from the optimal bond geometry; once the system becomes metallic, double

exchange causes the sudden increase in T_C to near room temperature.

According to our microscopic picture of magnetism and electronic correlations in CrGeTe_3 , both electron doping and hole doping induces double exchange mediated near room-temperature ferromagnetism: electron doping via chemical intercalation [90] or electrostatic gating [30] and hole doping by irradiation [94] or the application of pressure. In the endeavour to design 2D room-temperature magnets, the doping of ferromagnetic van der Waals materials will play an important role, and our study shows how the often invoked double-exchange mechanism can be experimentally substantiated.

Acknowledgments. H.O.J. acknowledges fruitful discussions with Han-Xiang Xu and Junya Otsuki. C.A.K. acknowledges financial support by the Deutsche Forschungsgemeinschaft (DFG), Germany, through Grant No. KU 1432/15-1. Part of the computation in this work has been done using the facilities of the Supercomputer Center, the Institute for Solid State Physics, the University of Tokyo.

- [1] J. Hwang, W. Ruan, Y. Chen, S. Tang, M. F. Crommie, Z.-X. Shen, and S.-K. Mo, Charge density waves in two-dimensional transition metal dichalcogenides, *Rep. Prog. Phys.* **87**, 044502 (2024).
- [2] S. Qiao, X. Li, N. Wang, W. Ruan, C. Ye, P. Cai, Z. Hao, H. Yao, X. Chen, J. Wu, Y. Wang, and Z. Liu, Mottness collapse in 1T-TaS_{2-x}Se_x transition-metal dichalcogenide: An interplay between localized and itinerant orbitals, *Phys. Rev. X* **7**, 041054 (2017).
- [3] H.-S. Kim, K. Haule, and D. Vanderbilt, Mott metal-insulator transitions in pressurized layered trichalcogenides, *Phys. Rev. Lett.* **123**, 236401 (2019).
- [4] Y. D. Wang, W. L. Yao, Z. M. Xin, T. T. Han, Z. G. Wang, L. Chen, C. Cai, Y. Li, and Y. Zhang, Band insulator to Mott insulator transition in 1T-TaS₂, *Nat. Commun.* **11**, 4215 (2020).
- [5] N. Tian, Z. Huang, B. G. Jang, S. Guo, Y.-J. Yan, J. Gao, Y. Yu, J. Hwang, C. Tang, M. Wang, X. Luo, Y. P. Sun, Z. Liu, D.-L. Feng, X. Chen, S.-K. Mo, M. Kim, Y.-W. Son, D. Shen,

- W. Ruan, and Y. Zhang, Dimensionality-driven metal to Mott insulator transition in two-dimensional 1T-TaSe₂, *Natl. Sci. Rev.* **11**, nwad144 (2024).
- [6] W. Shi, J. Ye, Y. Zhang, R. Suzuki, M. Yoshida, J. Miyazaki, N. Inoue, Y. Saito, and Y. Iwasa, Superconductivity series in transition metal dichalcogenides by ionic gating, *Sci. Rep.* **5**, 12534 (2015).
- [7] Y. Qi, P. G. Naumov, M. N. Ali, C. R. Rajamathi, W. Schnelle, O. Barkalov, M. Hanfland, S.-C. Wu, C. Shekhar, Y. Sun, V. Stüß, M. Schmidt, U. Schwarz, E. Pippel, P. Werner, R. Hillebrand, T. Förster, E. Kampert, S. Parkin, R. J. Cava *et al.*, Superconductivity in Weyl semimetal candidate MoTe₂, *Nat. Commun.* **7**, 11038 (2016).
- [8] B. Wang, Y. Liu, K. Ishigaki, K. Matsubayashi, J. Cheng, W. Lu, Y. Sun, and Y. Uwatoko, Pressure-induced bulk superconductivity in a layered transition-metal dichalcogenide 1T-tantalum selenide, *Phys. Rev. B* **95**, 220501(R) (2017).
- [9] M. M. Otrokov, I. I. Klimovskikh, H. Bentmann, D. Estyunin, A. Zeugner, Z. S. Aliev, S. Gaß, A. U. B. Wolter, A. V. Koroleva, A. M. Shikin, M. Blanco-Rey, M. Hoffmann, I. P. Rusinov, A. Y. Vyazovskaya, S. V. Eremeev, Y. M. Koroteev, V. M. Kuznetsov, F. Freyse, J. Sánchez-Barriga, I. R. Amiraslanov *et al.*, Prediction and observation of an antiferromagnetic topological insulator, *Nature (London)* **576**, 416 (2019).
- [10] J. Li, Y. Li, S. Du, Z. Wang, B.-L. Gu, S.-C. Zhang, K. He, W. Duan, and Y. Xu, Intrinsic magnetic topological insulators in van der Waals layered MnBi₂Te₄-family materials, *Sci. Adv.* **5**, eaaw5685 (2019).
- [11] H. Li, S.-Y. Gao, S.-F. Duan, Y.-F. Xu, K.-J. Zhu, S.-J. Tian, J.-C. Gao, W.-H. Fan, Z.-C. Rao, J.-R. Huang, J.-J. Li, D.-Y. Yan, Z.-T. Liu, W.-L. Liu, Y.-B. Huang, Y.-L. Li, Y. Liu, G.-B. Zhang, P. Zhang *et al.*, Dirac surface states in intrinsic magnetic topological insulators EuSn₂As₂ and MnBi_{2n}Te_{3n+1}, *Phys. Rev. X* **9**, 041039 (2019).
- [12] Y. Deng, Y. Yu, M. Z. Shi, Z. Guo, Z. Xu, J. Wang, X. H. Chen, and Y. Zhang, Quantum anomalous Hall effect in intrinsic magnetic topological insulator MnBi₂Te₄, *Science* **367**, 895 (2020).
- [13] B. Q. Lv, N. Xu, H. M. Weng, J. Z. Ma, P. Richard, X. C. Huang, L. X. Zhao, G. F. Chen, C. E. Matt, F. Bisti, V. N. Strocov, J. Mesot, Z. Fang, X. Dai, T. Qian, M. Shi, and H. Ding, Observation of Weyl nodes in TaAs, *Nat. Phys.* **11**, 724 (2015).
- [14] S.-Y. Xu, I. Belopolski, N. Alidoust, M. Neupane, G. Bian, C. Zhang, R. Sankar, G. Chang, Z. Yuan, C.-C. Lee, S.-M. Huang, H. Zheng, J. Ma, D. S. Sanchez, B. Wang, A. Bansil, F. Chou, P. P. Shibayev, H. Lin, S. Jia, and M. Z. Hasan, Discovery of a Weyl fermion semimetal and topological Fermi arcs, *Science* **349**, 613 (2015).
- [15] Q. Lu, P. V. S. Reddy, H. Jeon, A. R. Mazza, M. Brahlek, W. Wu, S. A. Yang, J. Cook, C. Conner, X. Zhang, A. Chakraborty, Y.-T. Yao, H.-J. Tien, C.-H. Tseng, P.-Y. Yang, S.-W. Lien, H. Lin, T.-C. Chiang, G. Vignale, A.-P. Li, Realization of a two-dimensional Weyl semimetal and topological Fermi strings, *Nat. Commun.* **15**, 6001 (2024).
- [16] K. Kim, J. Seo, E. Lee, K.-T. Ko, B. S. Kim, B. G. Jang, J. M. Ok, J. Lee, Y. J. Jo, W. Kang, J. H. Shim, C. Kim, H. W. Yeom, B. Il Min, B.-J. Yang, and J. S. Kim, Large anomalous Hall current induced by topological nodal lines in a ferromagnetic van der Waals semimetal, *Nat. Mater.* **17**, 794 (2018).
- [17] Q. Wang, Y. Xu, R. Lou, Z. Liu, M. Li, Y. Huang, D. Shen, H. Weng, S. Wang, and H. Lei, Large intrinsic anomalous Hall effect in half-metallic ferromagnet Co₃Sn₂S₂ with magnetic Weyl fermions, *Nat. Commun.* **9**, 3681 (2018).
- [18] C. Yun, H. Guo, Z. Lin, L. Peng, Z. Liang, M. Meng, B. Zhang, Z. Zhao, L. Wang, Y. Ma, Y. Liu, W. Li, S. Ning, Y. Hou, J. Yang, and Z. Luo, Efficient current-induced spin torques and field-free magnetization switching in a room-temperature van der Waals magnet, *Sci. Adv.* **9**, eadj3955 (2023).
- [19] Q. Wang, Y. Zeng, K. Yuan, Q. Zeng, P. Gu, X. Xu, H. Wang, Z. Han, K. Nomura, W. Wang, E. Liu, Y. Hou, and Y. Ye, Magnetism modulation in Co₃Sn₂S₂ by current-assisted domain wall motion, *Nat. Electron.* **6**, 119 (2023).
- [20] F. Zhu, L. Zhang, X. Wang, F. J. dos Santos, J. Song, T. Mueller, K. Schmalzl, W. F. Schmidt, A. Ivanov, J. T. Park, J. Xu, J. Ma, S. Lounis, S. Y. Blügel, Mokrousov, Y. Su, and T. Brückel, Topological magnon insulators in two-dimensional van der Waals ferromagnets CrSiTe₃ and CrGeTe₃: Toward intrinsic gap-tunability, *Sci. Adv.* **7**, eabi7532 (2021).
- [21] J. Luo, S. Li, Z. Ye, R. Xu, H. Yan, J. Zhang, G. Ye, L. Chen, D. Hu, X. Teng, W. A. Smith, B. I. Yakobson, P. Dai, A. H. Nevidomskyy, R. He, and H. Zhu, Evidence for topological magnon-phonon hybridization in a 2D antiferromagnet down to the monolayer limit, *Nano Lett.* **23**, 2023 (2023).
- [22] F. Zhuo, J. Kang, A. Manchon, and Z. Cheng, Topological phases in magnonics, *Adv. Phys. Res.* **4**, 2300054 (2024).
- [23] C. Gong, L. Li, Z. Li, H. Ji, A. Stern, Y. Xia, T. Cao, W. Bao, C. Wang, Y. Wang, Z. Q. Qiu, R. J. Cava, S. G. Louie, J. Xia, and X. Zhang, Discovery of intrinsic ferromagnetism in two-dimensional van der Waals crystals, *Nature (London)* **546**, 265 (2017).
- [24] K. S. Burch, D. Mandrus, and J.-G. Park, Magnetism in two-dimensional van der Waals materials, *Nature (London)* **563**, 47 (2018).
- [25] X. Qian, J. Liu, L. Fu, and J. Li, Quantum spin Hall effect in two-dimensional transition metal dichalcogenides, *Science* **346**, 1344 (2014).
- [26] M. A. Cazalilla, H. Ochoa, and F. Guinea, Quantum spin Hall effect in two-dimensional crystals of transition-metal dichalcogenides, *Phys. Rev. Lett.* **113**, 077201 (2014).
- [27] Y. Deng, Y. Yu, Y. Song, J. Zhang, N. Z. Wang, Z. Sun, Y. Yi, Y. Z. Wu, S. Wu, J. Zhu, J. Wang, X. H. Chen, and Y. Zhang, Gate-tunable room-temperature ferromagnetism in two-dimensional Fe₃GeTe₂, *Nature (London)* **563**, 94 (2018).
- [28] Z. Wang, T. Zhang, M. Ding, B. Dong, Y. Li, M. Chen, X. Li, J. Huang, H. Wang, X. Zhao, Y. Li, D. Li, C. Jia, L. Sun, H. Guo, Y. Ye, D. Sun, Y. Chen, T. Yang, J. Zhang, S. Ono, Z. Han, and Z. Zhang, Electric-field control of magnetism in a few-layered van der Waals ferromagnetic semiconductor, *Nat. Nanotechnol.* **13**, 554 (2018).
- [29] C. Gong and X. Zhang, Two-dimensional magnetic crystals and emergent heterostructure devices, *Science* **363**, eaav4450 (2019).
- [30] I. A. Verzhbitskiy, H. Kurebayashi, H. Cheng, J. Zhou, S. Khan, Y. P. Feng, and G. Eda, Controlling the magnetic anisotropy in Cr₂Ge₂Te₆ by electrostatic gating, *Nat. Electron.* **3**, 460 (2020).

- [31] M.-W. Lin, H. L. Zhuang, J. Yan, T. Z. Ward, A. A. Puretzky, C. M. Rouleau, Z. Gai, L. Liang, V. Meunier, B. G. Sumpter, P. Ganesh, P. R. C. Kent, D. B. Geohegan, D. G. Mandrus, and K. Xiao, Ultrathin nanosheets of CrGeTe₃: a semiconducting two-dimensional ferromagnetic material, *J. Mater. Chem. C* **4**, 315 (2016).
- [32] B. Liu, Y. Zou, L. Zhang, S. Zhou, Z. Wang, W. Wang, Z. Qu, and Y. Zhang, Critical behavior of the quasi-two-dimensional semiconducting ferromagnet CrSiTe₃, *Sci. Rep.* **6**, 33873 (2016).
- [33] W. Cai, H. Sun, W. Xia, C. Wu, Y. Liu, H. Liu, Y. Gong, D.-X. Yao, Y. Guo, and M. Wang, Pressure-induced superconductivity and structural transition in ferromagnetic CrSiTe₃, *Phys. Rev. B* **102**, 144525 (2020).
- [34] V. Carteaux, D. Brunet, G. Ouvrard, and G. Andre, Crystallographic, magnetic and electronic structures of a new layered ferromagnetic compound Cr₂Ge₂Te₆, *J. Phys.: Condens. Matter* **7**, 69 (1995).
- [35] H. Ji, R. A. Stokes, L. D. Alegria, E. C. Blomberg, M. A. Tanatar, A. Reijnders, L. M. Schoop, T. Liang, R. Prozorov, K. S. Burch, N. P. Ong, J. R. Petta, and R. J. Cava, A ferromagnetic insulating substrate for the epitaxial growth of topological insulators, *J. Appl. Phys.* **114**, 114907 (2013).
- [36] See Supplemental Material at <http://link.aps.org/supplemental/10.1103/PhysRevB.111.L140402> for further information on the sample preparation and characterization, crystal structure, low-temperature high-pressure infrared reflectivity measurements, analysis of reflectivity and optical conductivity spectra, and additional experimental and theoretical results.
- [37] D. Bhoi, J. Gouchi, N. Hiraoka, Y. Zhang, N. Ogita, T. Hasegawa, K. Kitagawa, H. Takagi, K. H. Kim, and Y. Uwatoko, Nearly room-temperature ferromagnetism in a pressure-induced correlated metallic state of the van der Waals insulator CrGeTe₃, *Phys. Rev. Lett.* **127**, 217203 (2021).
- [38] M. D. Watson, I. Marković, F. Mazzola, A. Rajan, E. A. Morales, D. M. Burn, T. Hesjedal, G. van der Laan, S. Mukherjee, T. K. Kim, C. Bigi, I. Vobornik, M. Ciomaga Hatnean, G. Balakrishnan, and P. D. C. King, Direct observation of the energy gain underpinning ferromagnetic superexchange in the electronic structure of CrGeTe₃, *Phys. Rev. B* **101**, 205125 (2020).
- [39] J. Zhang, X. Cai, W. Xia, A. Liang, J. Huang, C. Wang, L. Yang, H. Yuan, Y. Chen, S. Zhang, Y. Guo, Z. Liu, and G. Li, Unveiling electronic correlation and the ferromagnetic superexchange mechanism in the van der Waals crystal CrSiTe₃, *Phys. Rev. Lett.* **123**, 047203 (2019).
- [40] H.-X. Xu, M. Shimizu, D. Guterding, J. Otsuki, and H. O. Jeschke, Pressure evolution of electronic structure and magnetism in the layered van der Waals ferromagnet CrGeTe₃, *Phys. Rev. B* **108**, 125142 (2023).
- [41] H. K. Mao, J. Xu, and P. M. Bell, Calibration of the ruby pressure gauge to 800 kbar under quasi-hydrostatic conditions, *J. Geophys. Res.* **91**, 4673 (1986).
- [42] K. Syassen, Ruby under pressure, *High Press. Res.* **28**, 75 (2008).
- [43] M. I. Eremets and Y. A. Timofeev, Miniature diamond anvil cell: Incorporating a new design for anvil alignment, *Rev. Sci. Instrum.* **63**, 3123 (1992).
- [44] J. Ebad-Allah, M. Krottenmüller, J. Hu, Y. L. Zhu, Z. Q. Mao, and C. A. Kuntscher, Infrared spectroscopy study of the nodal-line semimetal candidate ZrSiTe under pressure: Hints for pressure-induced phase transitions, *Phys. Rev. B* **99**, 245133 (2019).
- [45] J. Ebad-Allah, S. Rojewski, M. Vöst, G. Eickerling, W. Scherer, E. Uykur, R. Sankar, L. Varrassi, C. Franchini, K.-H. Ahn, J. Kuneš, and C. A. Kuntscher, Pressure-induced excitations in the out-of-plane optical response of the nodal-line semimetal ZrSiS, *Phys. Rev. Lett.* **127**, 076402 (2021).
- [46] J. Ebad-Allah, S. Rojewski, Y. L. Zhu, Z. Q. Mao, and C. A. Kuntscher, In-plane and out-of-plane optical response of the nodal-line semimetals ZrGeS and ZrGeSe, *Phys. Rev. B* **106**, 075143 (2022).
- [47] D. B. Tanner, Use of x-ray scattering functions in Kramers-Kronig analysis of reflectance, *Phys. Rev. B* **91**, 035123 (2015).
- [48] Y. Lu, H. Kono, T. Larkin, A. Rost, T. Takayama, A. V. Boris, B. Keimer, and H. Takagi, Zero-gap semiconductor to excitonic insulator transition in Ta₂NiSe₅, *Nat. Commun.* **8**, 14408 (2017).
- [49] E. Uykur, R. Sankar, D. Schmitz, and C. A. Kuntscher, Optical spectroscopy study on pressure-induced phase transitions in the three-dimensional Dirac semimetal Cd₃As₂, *Phys. Rev. B* **97**, 195134 (2018).
- [50] R. Yang, M. Corasaniti, L. Wu, Q. Du, Y. Zhu, C. Petrovic, and L. Degiorgi, Ingredients for enhanced thermoelectric power at cryotemperatures in the correlated semiconductor CoSbS revealed by its optical response, *Phys. Rev. B* **103**, L161111 (2021).
- [51] M. Köpf, S. H. Lee, Z. Q. Mao, and C. A. Kuntscher, Optical study of the charge dynamics evolution in the topological insulators MnBi₂Te₄ and Mn(Bi_{0.74}Sb_{0.26})₂Te₄ under high pressure, *Phys. Rev. B* **109**, 245124 (2024).
- [52] K. Koepernik and H. Eschrig, Full-potential nonorthogonal local-orbital minimum-basis band-structure scheme, *Phys. Rev. B* **59**, 1743 (1999).
- [53] J. P. Perdew, K. Burke, and M. Ernzerhof, Generalized gradient approximation made simple, *Phys. Rev. Lett.* **77**, 3865 (1996).
- [54] Z. Yu, W. Xia, K. Xu, M. Xu, H. Wang, X. Wang, N. Yu, Z. Zou, J. Zhao, L. Wang, X. Miao, and Y. Guo, Pressure-induced structural phase transition and a special amorphization phase of two-dimensional ferromagnetic semiconductor Cr₂Ge₂Te₆, *J. Phys. Chem. C* **123**, 13885 (2019).
- [55] Y. Fang, S. Wu, Z.-Z. Zhu, and G.-Y. Guo, Large magneto-optical effects and magnetic anisotropy energy in two-dimensional Cr₂Ge₂Te₆, *Phys. Rev. B* **98**, 125416 (2018).
- [56] H. Shinaoka, J. Otsuki, M. Kawamura, N. Takemori, and K. Yoshimi, DCORE: Integrated DMFT software for correlated electrons, *SciPost Phys.* **10**, 117 (2021).
- [57] P. Werner, A. Comanac, L. de' Medici, M. Troyer, and A. J. Millis, Continuous-time solver for quantum impurity models, *Phys. Rev. Lett.* **97**, 076405 (2006).
- [58] E. Gull, A. J. Millis, A. I. Lichtenstein, A. N. Rubtsov, M. Troyer, and P. Werner, Continuous-time monte carlo methods for quantum impurity models, *Rev. Mod. Phys.* **83**, 349 (2011).
- [59] J. Otsuki, K. Yoshimi, H. Shinaoka, and H. O. Jeschke, Multipolar ordering from dynamical mean field theory with application to CeB₆, *Phys. Rev. B* **110**, 035104 (2024).
- [60] M. Aichhorn, L. Pourovskii, P. Seth, V. Vildosola, M. Zingl, O. E. Peil, X. Deng, J. Mravlje, G. J. Kraberger, C. Martins,

- M. Ferrero, and O. Parcollet, TRIQS/DFTTools: A TRIQS application for *ab initio* calculations of correlated materials, *Comput. Phys. Commun.* **204**, 200 (2016).
- [61] <https://github.com/j-otsuki/ethyb>
- [62] T. J. Kim, S. Ryee, M. J. Han, and S. Choi, Dynamical mean-field study of vanadium diselenide monolayer ferromagnetism, *2D Mater.* **7**, 035023 (2020).
- [63] H. Fujiwara, K. Terashima, J. Otsuki, N. Takemori, H. O. Jeschke, T. Wakita, Y. Yano, W. Hosoda, N. Kataoka, A. Teruya, M. Kakihana, M. Hedo, T. Nakama, Y. Ônuki, K. Yaji, A. Harasawa, K. Kuroda, S. Shin, K. Horiba, H. Kumigashira *et al.*, Anomalously large spin-dependent electron correlation in the nearly half-metallic ferromagnet CoS₂, *Phys. Rev. B* **106**, 085114 (2022).
- [64] B. G. Jang, G. Han, I. Park, D. Kim, Y. Y. Koh, Y. Kim, W. Kyung, H.-D. Kim, C.-M. Cheng, K.-D. Tsuei, K. D. Lee, N. Hur, J. H. Shim, C. Kim, and G. Kotliar, Direct observation of kink evolution due to Hund's coupling on approach to metal-insulator transition in NiS_{2-x}Se_x, *Nat. Commun.* **12**, 1208 (2021).
- [65] Y. Wang, C.-J. Kang, H. Miao, and G. Kotliar, Hund's metal physics: From SrNiO₂ to LaNiO₂, *Phys. Rev. B* **102**, 161118(R) (2020).
- [66] I. Leonov, S. L. Skornyakov, and S. Y. Savrasov, Lifshitz transition and frustration of magnetic moments in infinite-layer NdNiO₂ upon hole doping, *Phys. Rev. B* **101**, 241108(R) (2020).
- [67] C.-J. Kang, J. Hong, and J. Kim, Dynamical mean-field theory study of a ferromagnetic CrI₃ monolayer, *J. Korean Phys. Soc.* **80**, 1071 (2022).
- [68] H. Kajueter, G. Kotliar, and G. Moeller, Doped Mott insulator: Results from mean-field theory, *Phys. Rev. B* **53**, 16214 (1996).
- [69] O. Parcollet and A. Georges, Non-Fermi-liquid regime of a doped Mott insulator, *Phys. Rev. B* **59**, 5341 (1999).
- [70] B. Kyung, S. S. Kancharla, D. Sénéchal, A.-M. S. Tremblay, M. Civelli, and G. Kotliar, Pseudogap induced by short-range spin correlations in a doped Mott insulator, *Phys. Rev. B* **73**, 165114 (2006).
- [71] D. E. Logan and M. R. Galpin, Mott insulators and the doping-induced Mott transition within DMFT: exact results for the one-band Hubbard model, *J. Phys.: Condens. Matter* **28**, 025601 (2016).
- [72] A. A. Katanin, A. P. Kampf, and V. Y. Irkhin, Anomalous self-energy and Fermi surface quasisplitting in the vicinity of a ferromagnetic instability, *Phys. Rev. B* **71**, 085105 (2005).
- [73] H. J. Vidberg and J. W. Serene, Solving the Eliashberg equations by means of N-point Padé approximants, *J. Low Temp. Phys.* **29**, 179 (1977).
- [74] J. Otsuki, M. Ohzeki, H. Shinaoka, and K. Yoshimi, Sparse modeling in quantum many-body problems, *J. Phys. Soc. Jpn.* **89**, 012001 (2020).
- [75] L.-F. Arsenault, P. Sémon, and A.-M. S. Tremblay, Benchmark of a modified iterated perturbation theory approach on the fcc lattice at strong coupling, *Phys. Rev. B* **86**, 085133 (2012).
- [76] H. Eschrig and K. Koepernik, Tight-binding models for the iron-based superconductors, *Phys. Rev. B* **80**, 104503 (2009).
- [77] C.-J. Kang and G. Kotliar, Optical properties of the infinite-layer La_{1-x}Sr_xNiO₂ and hidden Hund's physics, *Phys. Rev. Lett.* **126**, 127401 (2021).
- [78] V. M. Pereira, J. M. B. Lopes dos Santos, E. V. Castro, and A. H. Castro-Neto, Double exchange model for magnetic hexaborides, *Phys. Rev. Lett.* **93**, 147202 (2004).
- [79] P. W. Anderson and H. Hasegawa, Considerations on double exchange, *Phys. Rev.* **100**, 675 (1955).
- [80] Y. Shao, A. N. Rudenko, J. Hu, Z. Sun, Y. Zhu, S. Moon, A. J. Millis, S. Yuan, A. I. Lichtenstein, D. Smirnov, Z. Q. Mao, M. I. Katsnelson, and D. N. Basov, Electronic correlations in nodal-line semimetals, *Nat. Phys.* **16**, 636 (2020).
- [81] L. Degiorgi, Electronic correlations in iron-pnictide superconductors and beyond: lessons learned from optics, *New J. Phys.* **13**, 023011 (2011).
- [82] M. M. Qazilbash, J. J. Hamlin, R. E. Baumbach, L. Zhang, D. J. Singh, M. B. Maple, and D. N. Basov, Electronic correlations in the iron pnictides, *Nat. Phys.* **5**, 647 (2009).
- [83] Y. F. Li, W. Wang, W. Guo, C. Y. Gu, H. Y. Sun, L. He, J. Zhou, Z. B. Gu, Y. F. Nie, and X. Q. Pan, Electronic structure of ferromagnetic semiconductor CrGeTe₃ by angle-resolved photoemission spectroscopy, *Phys. Rev. B* **98**, 125127 (2018).
- [84] M. Suzuki, B. Gao, K. Koshiishi, S. Nakata, K. Hagiwara, C. Lin, Y. X. Wan, H. Kumigashira, K. Ono, S. Kang, S. Kang, J. Yu, M. Kobayashi, S.-W. Cheong, and A. Fujimori, Coulomb-interaction effect on the two-dimensional electronic structure of the van der Waals ferromagnet Cr₂Ge₂Te₆, *Phys. Rev. B* **99**, 161401(R) (2019).
- [85] Y. Liu and C. Petrovic, Critical behavior of quasi-two-dimensional semiconducting ferromagnet Cr₂Ge₂Te₆, *Phys. Rev. B* **96**, 054406 (2017).
- [86] S. Spachmann, A. Elghandour, S. Selter, B. Büchner, S. Aswartham, and R. Klingeler, Strong effects of uniaxial pressure and short-range correlations in Cr₂Ge₂Te₆, *Phys. Rev. Res.* **4**, L022040 (2022).
- [87] X. Pan, B. Xin, H. Zeng, P. Cheng, T. Ye, D. Yao, E. Xue, J. Ding, and W.-H. Wang, Pressure-induced structural phase transition and enhanced interlayer coupling in two-dimensional ferromagnet CrSiTe₃, *J. Phys. Chem. Lett.* **14**, 3320 (2023).
- [88] M. Krottenmüller, M. Vöst, N. Unglert, J. Ebad-Allah, G. Eickerling, D. Volkmer, J. Hu, Y. L. Zhu, Z. Q. Mao, W. Scherer, and C. A. Kuntscher, Indications for Lifshitz transitions in the nodal-line semimetal ZrSiTe induced by interlayer interaction, *Phys. Rev. B* **101**, 081108(R) (2020).
- [89] Y. Sun, R. C. Xiao, G. T. Lin, R. R. Zhang, L. S. Ling, Z. W. Ma, X. Luo, W. J. Lu, Y. P. Sun, and Z. G. Sheng, Effects of hydrostatic pressure on spin-lattice coupling in two-dimensional ferromagnetic Cr₂Ge₂Te₆, *Appl. Phys. Lett.* **112**, 072409 (2018).
- [90] N. Wang, H. Tang, M. Shi, H. Zhang, W. Zhuo, D. Liu, F. Meng, L. Ma, J. Ying, L. Zou, Z. Sun, and X. Chen, Transition from ferromagnetic semiconductor to ferromagnetic metal with enhanced Curie temperature in Cr₂Ge₂Te₆ via organic ion intercalation, *J. Am. Chem. Soc.* **141**, 17166 (2019).
- [91] H. Idzuchi, A. E. Llacsahuanga Alleca, A. K. A. Lu, M. Saito, S. Das, J. F. Ribeiro, M. Houssa, R. Meng, K. Inoue, X.-C. Pan, K. Tanigaki, Y. Ikuhara, T. Nakanishi, and Y. P. Chen, Enhanced ferromagnetism in an artificially stretched lattice in quasi-two-dimensional Cr₂Ge₂Te₆, *Phys. Rev. B* **111**, L020402 (2025).

- [92] B. H. Zhang, Y. S. Hou, Z. Wang, and R. Q. Wu, First-principles studies of spin-phonon coupling in monolayer $\text{Cr}_2\text{Ge}_2\text{Te}_6$, *Phys. Rev. B* **100**, 224427 (2019).
- [93] X.-J. Dong, J.-Y. You, Z. Zhang, B. Gu, and G. Su, Great enhancement of Curie temperature and magnetic anisotropy in two-dimensional van der Waals magnetic semiconductor heterostructures, *Phys. Rev. B* **102**, 144443 (2020).
- [94] S. Zhang, K. Harii, T. Yokouchi, S. Okayasu, and Y. Shiomi, Amorphous ferromagnetic metal in van der Waals materials, *Adv. Electron. Mater.* **10**, 2300609 (2024).
- [95] R. Matsumoto, S. Yamamoto, K. Terashima, K. Yamane, and Y. Takano, Electrical transport properties of van der Waals insulator CrGeTe_3 under extremely high pressure up to 52 GPa, *J. Phys. Soc. Jpn.* **93**, 044710 (2024).
- [96] G. Scharf, D. Guterding, B. Hen, P. M. Sarte, B. R. Ortiz, G. K. Rozenberg, T. Holder, S. D. Wilson, H. O. Jeschke, and A. Ron, Pressure tuning of intrinsic and extrinsic sources to the anomalous Hall effect in CrGeTe_3 , *Phys. Rev. Res.* **7**, 013127 (2025).
- [97] L. D. Casto, A. J. Clune, M. O. Yokosuk, J. L. Musfeldt, T. J. Williams, H. L. Zhuang, M.-W. Lin, K. Xiao, R. G. Hennig, B. C. Sales, J.-Q. Yan, and D. Mandrus, Strong spin-lattice coupling in CrSiTe_3 , *APL Mater.* **3**, 041515 (2015).
- [98] J.-H. Park, C. T. Chen, S.-W. Cheong, W. Bao, G. Meigs, V. Chakarian, and Y. U. Idzerda, Electronic aspects of the ferromagnetic transition in manganese perovskites, *Phys. Rev. Lett.* **76**, 4215 (1996).
- [99] D. D. Sarma, N. Shanthi, S. R. Krishnakumar, T. Saitoh, T. Mizokawa, A. Sekiyama, K. Kobayashi, A. Fujimori, E. Weschke, R. Meier, G. Kaindl, Y. Takeda, and M. Takano, Temperature-dependent photoemission spectral weight in $\text{La}_{0.6}\text{Sr}_{0.4}\text{MnO}_3$, *Phys. Rev. B* **53**, 6873 (1996).
- [100] T. Saitoh, A. Sekiyama, K. Kobayashi, T. Mizokawa, A. Fujimori, D. D. Sarma, Y. Takeda, and M. Takano, Temperature-dependent valence-band photoemission spectra of $\text{La}_{1-x}\text{Sr}_x\text{MnO}_3$, *Phys. Rev. B* **56**, 8836 (1997).
- [101] L. Degiorgi, E. Felder, H. R. Ott, J. L. Sarrao, and Z. Fisk, Low-temperature anomalies and ferromagnetism of EuB_6 , *Phys. Rev. Lett.* **79**, 5134 (1997).
- [102] J. Kim, Y.-J. Kim, J. Kuneš, B. K. Cho, and E. J. Choi, Optical spectroscopy and electronic band structure of ferromagnetic EuB_6 , *Phys. Rev. B* **78**, 165120 (2008).